Entanglement transfer via Chiral and Continuous-Time Quantum Walks on a Triangular Chain

Utku Sağlam

Department of Physics, 1150 University Avenue, University of Wisconsin at Madison, Madison, Wisconsin 53706, USA

Mauro Paternostro

Centre for Theoretical Atomic, Molecular, and Optical Physics, School of Mathematics and Physics, Queen's University, Belfast BT7 1NN, United Kingdom

Özgür E. Müstecaplıoğlu

Department of Physics, Koç University, Sarıyer, İstanbul, 34450, Turkey

TÜBİTAK Research Institute for Fundamental Sciences, 41470 Gebze, Turkey

Abstract

We investigate the chiral quantum walk (CQW) as a mechanism for an entanglement transfer on a triangular chain structure. We specifically consider two-site spatially entangled cases in short-time and long-time regimes. Using the concurrence as an entanglement measure; fidelity, and the Bures distance as the measure of the quality of the state transfer, we evaluate the success of the entanglement transfer. We compare the entangled state transfer time and quality in CQW against a continuous-time quantum random walk. We also observe the effect of mixed states on the entanglement transfer quality.

Keywords: Quantum Walks, Chiral Quantum Walks, Entanglement Transfer

1. Introduction

Fast and accurate transmission of quantum states through communication or computation networks is a critical objective for quantum technologies [1, 2, 3].

Email addresses: usaglam@wisc.edu (Utku Sağlam), m.paternostro@qub.ac.uk (Mauro Paternostro), omustecap@ku.edu.tr (Özgür E. Müstecaplıoğlu)

September 22, 2022

Proposed schemes to achieve this goal consider engineered couplings between the network sites [4, 5, 6, 7, 8, 9, 10, 11, 12, 13], external fields [14, 15, 16, 17], weak measurements [18, 19], or transport in noisy environments of biological or synthetic systems [20, 21, 22, 23, 24]. Such methods are challenging to implement in practice for quantum entanglement transfer, due to quantum decoherence and disorder [25, 26].

Pretty-good State Transfer (PGST) can be achieved on dual-spin chains [27], spin chains with weakly coupled endpoints [7, 28, 29, 30, 31], and projective measurements [32] with Quantum Walk (QW) schemes. Continuous time quantum walk (CTQW) is a paradigmatic model of quantum transport [33, 34]. Both discrete- [35, 36] and continuous-time [37, 38, 39, 40] quantum walks have been discussed for PGST. CTQW can be made one way by taking complex-valued couplings, which is called a chiral quantum walk (CQW) [41, 42, 43]. Chirality emerges due to the breaking of time-reversal symmetry (TRS) [44], and it provides a significant boost to transport speed [41].

High-dimensional entanglement (entanglement in high-dimensional degrees of freedom, such as spatial path modes) is advantageous in quantum communication [45] and quantum superdense coding [46, 47, 48]. The perfect state transfer (PST) in spin chains paves the way for the creation of required entangled states and logic gate structures for quantum computation and quantum information [49, 50]. High-dimensional entangled states can be produced by repeatedly generating the entanglement in a low-dimensional system and transferring these to a higher dimensional one [51]. Our first goal is to explore if CQW can be used to transmit two-dimensional quantum entangled states; what are the possible advantages it may offer? In addition, we ask if and to which extent CTQW can be used in place of CQW with the same chiral properties. CTQW can be easier to implement than CQW. For that aim, we identify the underlying physics of the chiral nature of QW in terms of quantum path interference, which can be controlled either via the phase in the initial state for CTQW or via the phase in complex hopping coefficients in CQW.

We specifically consider CQW on a linear spin chain of equilateral triangles, as shown in Fig. 1, which is the simplest graph that allows for so-called probability time symmetry (PTS) breaking [42]. A walker can transfer from one node to any other neighboring site on the triangular plaquette by passing through either one or two edges. We consider a uniform complex coupling between the nearest-neighbor sites. Due to the path length difference between the odd and even number of edges traveled, and phases of the complex couplings, interference can enhance the transfer rate. Path interference in the context of quantum walk means

that the relative phase between different trajectories the particle can traverse from one site to another one can give constructive or destructive interference effects in the site-to-site probability transfer. By using special graph topologies, complex-valued site-to-site couplings, or specific initial states, one can use path interference to break the PTS. CTQW can only utilize the latter, initial states with specific phases to exploit quantum interference while CQW can use both the freedom to choose the initial state and complex hopping coefficients to break PTS.

The spatial entanglement can be defined in the site basis for quantum walks [52, 53]. We assume a particle (we call a spin excitation as a particle) in a Bell-like spatially entangled state of two sites injected into the chain from the left. The quality of the transfer is examined by calculating the density matrix, concurrence [54], fidelity, and Bures distances explicitly [55, 56, 57]. We have also numerically confirmed that the entanglement state transfer time linearly scales with the chain size [58, 59, 60].

The triangular chain lattice can be realized in superconducting circuits [61, 62], trapped ions [63], NMR systems [42], photonic and spin waveguides [64], and in optical lattices [65]. In the case of optical lattices, complex edge weights could be introduced with the help of artificial gauge fields [66, 67], nitrogen-vacancy centers in diamonds [68] or with plasmonic non-Hermitian coupled waveguides [69].

This paper is organized as follows. We introduce the CQW on a triangular chain model by presenting the adjacency matrix and present the associated Hamiltonian model with complex hopping rates in Sec. 2. Our results are given in Sec. 3 in five subsections. PTS breaking and entanglement transfer in CTQW and CQW on a triangular chain are discussed in Sec. 3.1 and Sec. 3.2, respectively. We conclude in Sec. 4.

2. CQW on a triangular chain

Typical quantum walks exhibit time-reversal symmetry (TRS) in transfer probabilities between sites n and m in forward (t) and backward ($-t$) times such that $P_{nm}(t) = P_{nm}(-t)$. CQWs break the TRS and allow for so-called "directionally biased" transport, $P_{nm}(t) \neq P_{mn}(t)$, in certain graph structures [42]. We consider CQW on a triangular chain of N vertices as shown in Fig. 1, which is a minimal configuration with PTS breaking for a quantum walk with a directional bias [42].

We will use the site basis $\{|i\rangle\}$, with $i = 1, ..., \mathrm{N}$ indicating which site is occupied such that $|i\rangle := |0_1, 0_2, .., 1_i, ..0_{\mathrm{N}}\rangle$. The set of coupled sites in a graph

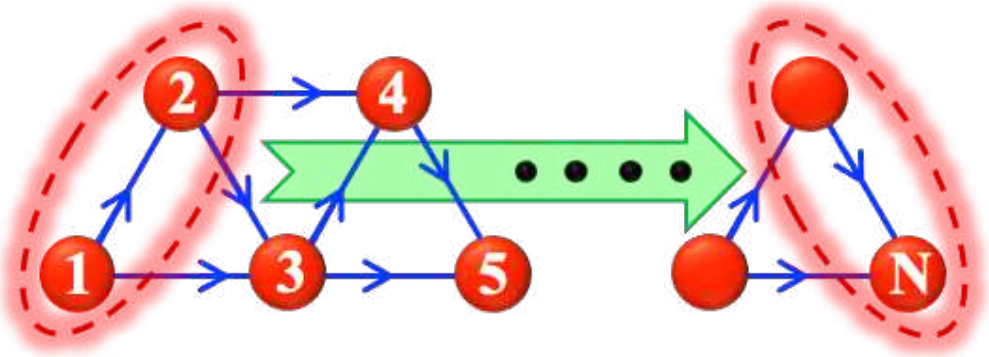


Figure 1: Graph of a linear chain with N vertices arranged in triangular plaquettes. Initially, the pair of sites 1 and 2 at the left end of the chain are entangled. The entangled state is transported to the rightmost pair of vertices ($N-1$ and N) after a chiral quantum walk. Arrows indicate the directed edges with complex weight factors, taken to be $+i$. In the opposite direction, the weight factors change phase and become $-i$. We have also examined transferring three-site entanglement from the leftmost plaquette ($1, 2$ and 3) to the right end of the chain.

determines the edges $e = (i, j)$, which can be described by the so-called adjacency matrix A [70, 71, 72, 73]. For a triangular chain of $N = 5$ sites, A is given by

$$A = \begin{bmatrix} 0 & 1 & 1 & 0 & 0 \\ 1 & 0 & 1 & 1 & 0 \\ 1 & 1 & 0 & 1 & 1 \\ 0 & 1 & 1 & 0 & 1 \\ 0 & 0 & 1 & 1 & 0 \end{bmatrix}. \tag{1}$$

Together with the degree matrix (For definitions of some graph theory terms see Appendix C) D for the self edges (i,i), A, determines the graph Laplacian $L = D - A$. Hamiltonian of the walk is given by the Hadamard product mentioned in the Appendix C, $H = J \circ L$, where J is the matrix of hopping rates (edge weights). We neglect the self energies; therefore, we will take $D = 0$ and write the Hamiltonian as

$$H = \sum_{nm} (J_{nm} A_{nm} |n\rangle\langle m| + J_{mn} A_{mn} |m\rangle\langle n|). \tag{2}$$

In contrast to CTQW where every J_{nm} is real-valued, CQW allows for complex edge weights, subject to $J_{mn} = J_{nm}^*$, so that the support graph of the walk

becomes a directed one (cf. Fig. 1). Specifically, we take

$$H = \begin{bmatrix} 0 & -\mathrm{i} & -\mathrm{i} & 0 & 0 \\ \mathrm{i} & 0 & -\mathrm{i} & -\mathrm{i} & 0 \\ \mathrm{i} & \mathrm{i} & 0 & -\mathrm{i} & -\mathrm{i} \\ 0 & \mathrm{i} & \mathrm{i} & 0 & -\mathrm{i} \\ 0 & 0 & \mathrm{i} & \mathrm{i} & 0 \end{bmatrix} \tag{3}$$

The choice of the phase $\theta_{nm} = \theta = \pi/2$ of complex hopping weights $J_{nm} = |J_{nm}| \exp(\mathrm{i}\theta_{nm})$ (with $n > m$) is based upon the general investigations of CQW [41] for a triangular plaquette. It is found that maximum bias in time asymmetry can be obtained at $\theta = \pi/2$ [41]. Remarkably, the spectrum of Hamiltonian with a phase of $\pi/2$ has an anti-symmetric structure

$$\begin{aligned} \Lambda_{1,2,3,4,5} = (&-\sqrt{\frac{1}{2}(7+\sqrt{37})}, -\sqrt{\frac{1}{2}(7-\sqrt{37})}, 0, \\ &\sqrt{\frac{1}{2}(7-\sqrt{37})}, \sqrt{\frac{1}{2}(7+\sqrt{37})}). \end{aligned} \tag{4}$$

We intuitively assume that a similar choice should yield efficient entanglement transfer along a linear chain of equilateral triangles, too. We numerically examined different choices and verified that our intuition is correct (Some typical results will be given in Sec. 3). The eigenstates corresponding to $\theta = \pi/2$ are given in Appendix B.

The evolution of the initial state of the system $\rho(0)$ is given by $\rho(t) = U\rho(0)U^\dagger$ where $U := \exp(\text{-i}Ht)$. We define the site states of the chain as $|1\rangle, ... |i\rangle$, where i's are the site numbers. Therefore, as the initial state, we consider a spatially entangled state $|\psi_{\text{spatial}}\rangle = (|1\rangle - \exp(i\phi)\,|2\rangle)/\sqrt{2}$ with the phase ϕ, of the leftmost sites of the chain and we aim to transfer the state to the right end of the chain.

Remarkably, even with initial superposition states on our linear triangular chain, could not yield PST (cf. Fig. 2). The graphs that can support PST require to be hermitian, circulant (C), and to have a non-degenerate spectrum, together with a flat eigenbasis [39]. Definitions of the graph theory terms we use are given in Appendix C. Alternatively, PST can still be achieved with a non-circulant graph that contains non-zero values on certain off-diagonal elements of its adjacency matrix [40]. From a practical point of view, implementing graph structures that have PST is challenging because of the sophisticated and usually numerous special connectivities of these graphs. Therefore, creating a simpler graph with

PGST can be more feasible in practice than using a graph with a PST. Since our proposed adjacency matrix is neither circulant nor has required non-zero off-diagonal elements, we do not expect any PST.

A fundamental difference between CQW and CTQW regarding the directional bias lies in how the transport bias is introduced. In CQW, the directional bias emerges by the differences in transition probabilities depending on the Hamiltonian regardless of the initial states to be transported. In CTQW, directional symmetry breaking is sensitive to the phase differences in the initial particle state in the (spatial) site basis. Intuitively, there is an interplay of path interference and the initial phase in CTQW in breaking PTS. The significance of the difference between the CQW and CTQW in such a directionally biased entanglement transfer is the ability of CQW to break PTS for any initial condition, while directionally biased entanglement transfer in CTQW happens only for certain initial states.

In this paper, we consider two time ranges to investigate the entanglement transfer dynamics. The first one, which we call the short-time regime, is to probe the first maximum of the entanglement measure (concurrence) or success fidelity of the state transfer. The second case is called the long-time regime, allowing multiple scatterings of the particle at the ends of the chain. The latter case is used to probe if more successful entanglement transfer is possible or not, at the cost of longer transfer times.

3. Results and Discussion

We will start with an examination of PTS-breaking in CTQW on the triangular chain. We do not need complex edge weights to break PTS in general. The essential physical mechanism behind PTS breaking is the quantum path interference, for which the required phase difference, or quantum coherence, can be injected into the initial state instead of the edges. Specifically, we consider a particle that is spatially entangled in two sites in the site basis,

$$|\psi_{\text{spatial}}(0)\rangle = \frac{1}{\sqrt{2}}(|1\rangle - \mathrm{e}^{\mathrm{i}\phi}\,|2\rangle) \tag{5}$$

on a regular triangular chain with real-valued hopping weights (we take $J_{nm} = 1$ for simplicity).

We want to transfer the input state to the end-sites of the structure. Ideally, we would like to achieve the target state $|\psi_{\text{target}}\rangle = (|4\rangle - \exp(\mathrm{i}\phi)\,|5\rangle)/\sqrt{2}$. To characterize the performance of the actual process, in addition to the fidelity of state transfer $|\,\langle\psi_{\text{target}}|\psi(t)\rangle\,|^2$, we quantify the entanglement transferred to the

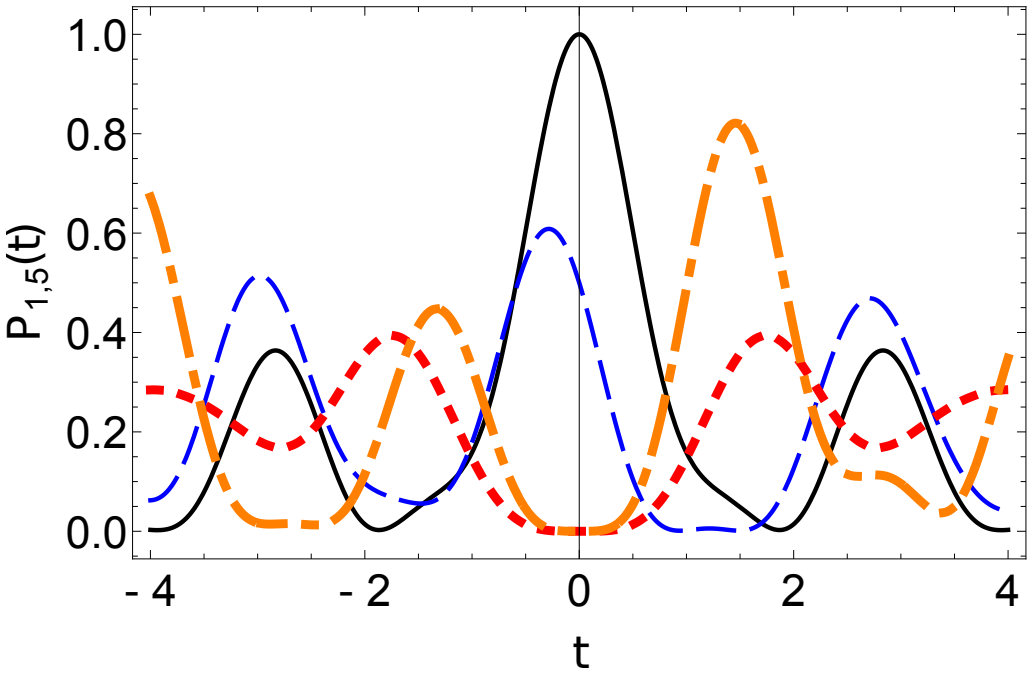


Figure 2: Time dependence of the occupation probabilities $P_{1,5}(t)$ of sites 1 and 5 of a triangular chain with 5 sites, where a particle makes CTQW. For an initially localized particle with an initial state $|1\rangle$, $P_1(t)$ and $P_5(t)$ are indicated by black, solid, and dotted, red curves, respectively. For a particle initially in a superposition state $|\psi(0)\rangle = (|1\rangle - \exp(\mathrm{i}\phi)\,|2\rangle)/\sqrt{2}$ with $\phi = 3\pi/4$, $P_1(t)$ and $P_5(t)$ are shown as dashed, blue and dot-dashed, orange curves, respectively.

end of the chain (sites 4 and 5). As we have only a single excitation, the initial state in Eq. (5) evolves into a state in the form

$$\begin{aligned} |\psi(t)\rangle = (A_1\,|100\rangle_{123} + A_2\,|010\rangle_{123} + A_3\,|001\rangle_{123})\,|00\rangle_{45} \\ + |000\rangle_{123}\,(A_4\,|10\rangle_{45} + A_5\,|01\rangle_{45})\,, \end{aligned} \tag{6}$$

where A_i are the time-dependent coefficients depending on the eigenvalues of the Hamiltonian of the QW.

Tracing out the states of the sites $1, 2$ and 3 in the density matrix $\rho(t) = |\psi(t)\rangle\,\langle\psi(t)|$, we find the reduced density matrix in the computational basis $|4\rangle\,|5\rangle = |00\rangle, |01\rangle, |10\rangle, |11\rangle$ for the sites 4 and 5 in the form

$$\rho_{4,5} = \begin{bmatrix} 1 - a_{44} - a_{55} & 0 & 0 & 0 \\ 0 & a_{44} & a_{45} & 0 \\ 0 & a_{45}^* & a_{55} & 0 \\ 0 & 0 & 0 & 0 \end{bmatrix}, \tag{7}$$

where $a_{ij} = A_i A_j^*$. The distribution of the zero elements, and hence the sparsity of the matrix, remains the same for any chain length.

We can quantify the pairwise entanglement using concurrence [54]. For a state ρ, concurrence is defined as

$$C(\rho) = \max(0, \lambda_1 - \lambda_2 - \lambda_3 - \lambda_4), \tag{8}$$

where $\tilde{\rho}$ is the spin-flipped state, and $\{\lambda_i\}$ is the set of eigenvalues of $R = (\rho^{1/2}\tilde{\rho}\rho^{1/2})^{1/2}$ arranged in non-increasing order. With this at hand, $C_{i=4,j=5}$ is found to take the form

$$C_{4,5} = 2\text{Max}\left(0, \sqrt{a_{44}a_{55}}, |a_{45}|\right). \tag{9}$$

Owing to the definition of a_{ij}, the concurrence $C_{4,5}$ can further be simplified to $C_{4,5} = 2|a_{45}|$. Note that this result can be extended to the matrices with arbitrary size associated with chains of length N, giving $C_{N-1,N} = 2|a_{N-1,N}|$.

Using the Hamiltonian matrix H in Eq. (3) and the initial state $\rho(0) = |\psi_{\text{spatial}}(0)\rangle \langle\psi_{\text{spatial}}(0)|$ in Eq. (5), with any ϕ, the dynamics of the entanglement between pairs of sites of the system can be calculated numerically for any value of t. We will also investigate the transport of the initial entangled Bell site-state from the sites 1 and 2 to sites 4 and 5 in CQW. We will perform the calculations for both CQW and CTQW cases separately. In the case of CTQW we use the initial state in Eq. (5).

3.1. PTS breaking and entanglement transfer in CTQW on a triangular chain

To appreciate the role of the initial phase in Eq. (5) on the state transfer and PTS breaking in CTQW on the triangular chain, let's start with the initial state $|\psi(0)\rangle = |1\rangle$. The occupation probabilities $P_i = \langle i|\rho(t)|i\rangle$ of the sites $i = 1$ (solid, black) and $i = 5$ (dotted, red) are shown in Fig. 2, where mirror symmetry in the behaviour of the probability distribution with respect to time can be seen. Transfer from the initially occupied site $|1\rangle$ to the rightmost site $|5\rangle$ is found to be weak (less than 45% at any time).

If we use the initial state given in Eq. (5) with the Adjacency matrix Eq. (1), in addition to being able to control path interference, PTS can be broken depending on the initial phase ϕ. We have numerically compared $P_5(t)$ for different ϕ and found that $\phi = 3\pi/4$ gives the largest occupation of site $|5\rangle$. Fig. 2 shows $P_1(t)$ (dotted, red) and $P_5(t)$ (dot-dashed, orange) for $\phi = 3\pi/4$, where time reversal asymmetry, $P(t) \neq P(-t)$ emerges. Population transfer is significantly enhanced using such a superposition state initially. We conclude that transferring a particle from the left end of the chain to a site at the right end is more successful by

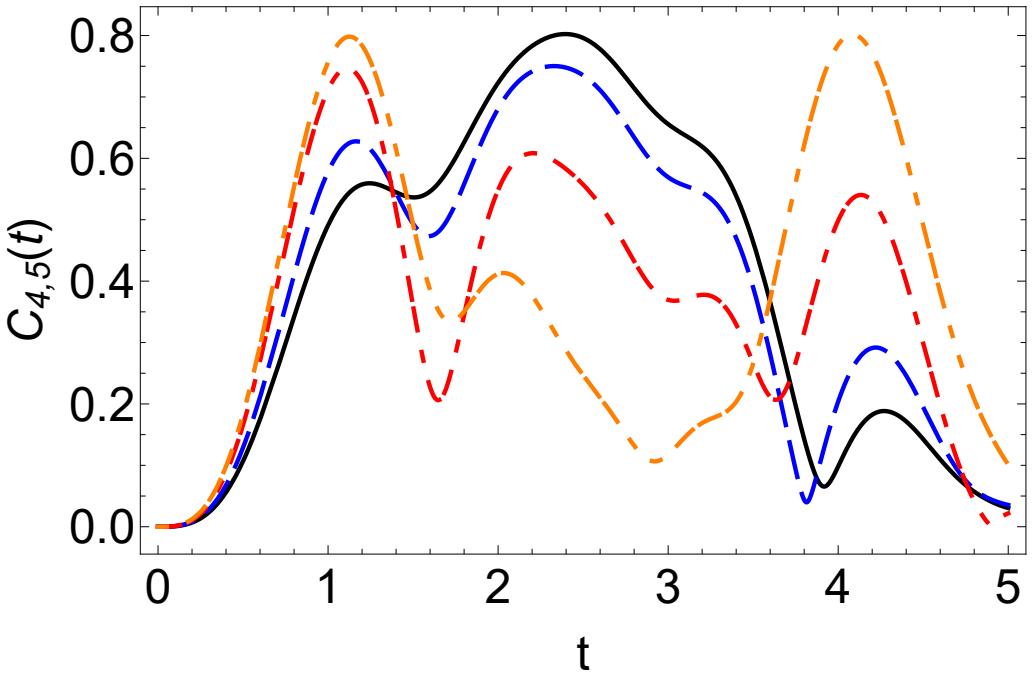


Figure 3: Time dependence of the concurrence $C_{4,5}(t)$ in the state of sites $|4\rangle$ and $|5\rangle$ for the initial state in Eq. (5) of a particle that makes CTQW on a triangular chain of $N = 5$ sites. Different curves stand for the initial states $|\psi(0)\rangle = (|1\rangle - \exp(\mathrm{i}\phi)\,|2\rangle)/\sqrt{2}$ with $\phi = \pi/4$ (solid, black), $\phi = \pm\pi/3$ (dashed, blue), $\phi = \pm\pi/2$ (dot-dashed, red), $\phi = \pm 3\pi/4$ (dotted, orange).

injecting the particle simultaneously at two sites with a certain quantum coherence relative to starting a well-localized particle at a single site. Let's now explore if similar advantages can be found in the entanglement transfer.

Fig. 3 shows that the concurrence is optimum for $\phi = \pm 3\pi/4$ with a value $C_{4,5}(1.12) \sim 0.8$. Therefore, for pairwise entanglement transfer, $\phi = 3\pi/4$ gives the most advantageous initial state. A natural question to ask is if there is a fundamental connection between the critical phase $\phi = 3\pi/4$ and PTS breaking in CTQW.

We can quantify the bias between the forward and backward time evolutions using the Bures distance between the states $\rho(t)$ and $\rho(-t)$. Bures distance is defined by [55, 56, 57]

$$D_B(\rho,\sigma)^2 = 2(1 - \sqrt{F(\rho,\sigma)}), \tag{10}$$

where

$$F(\rho,\sigma) = [\mathrm{Tr}(\sqrt{\sqrt{\rho}\sigma\sqrt{\rho}})]^2 \tag{11}$$

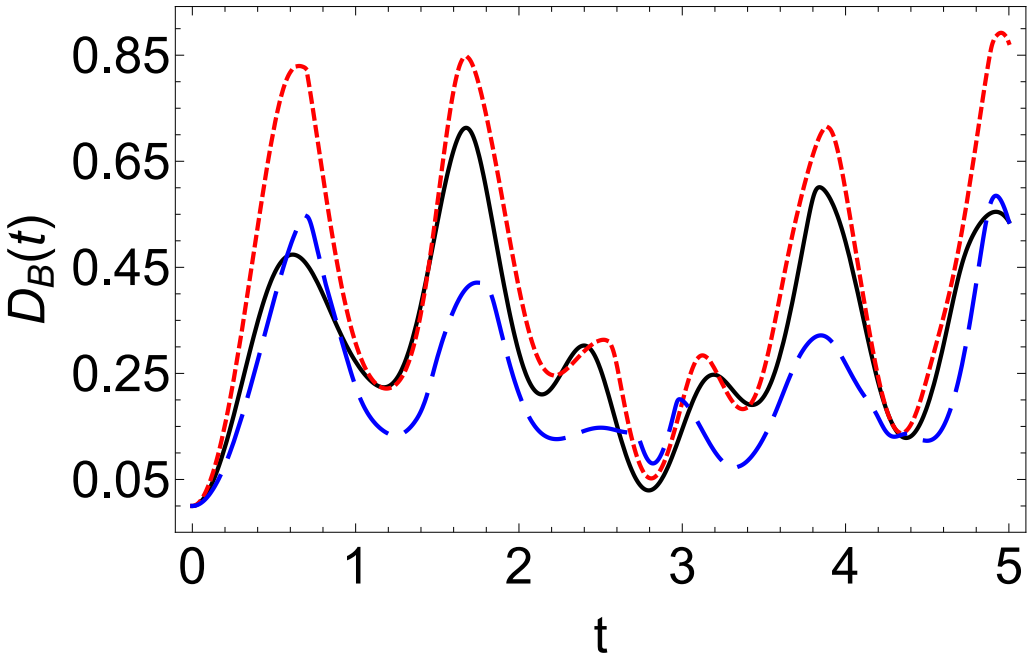


Figure 4: Time dependence of the Bures distance between the diagonal elements of the forward and backward evolved density matrices $\rho(t)$ and $\rho(-t)$, for a CTQW on a triangular chain. The curves are for the phases ϕ in the initial state $|\psi(0)\rangle = (|1\rangle - \exp(\mathrm{i}\phi)\,|2\rangle)/\sqrt{2}$ with $\phi = \pm\pi/3$ (solid, black), $\phi = \pm\pi/2$ (dotted, red) and $\phi = \pm 3\pi/4$ (dashed blue). The Bures distance for the phases $\phi = 0$ and $\phi = \pm\pi$ are zero.

is the fidelity [74].

In Fig. 4, we only use the diagonal elements of $\rho(t)$ and $\rho(-t)$ while calculating the Bures distance $D_B(t)$ for different ϕ's. As the probability information is maintained on the diagonal elements of the density matrices, the off-diagonal elements are discarded to demonstrate the broken PTS conditions more clearly. For the phases 0 and $\pm\pi$ the PTS is not broken and the Bures distance is zero. The largest bias in forward and backward time evolution is found for $\phi = \pi/2$, which is different from the critical phase $\phi = 3\pi/4$ for optimum population and entanglement transfer in CTQW over a triangular chain. We conclude that the CTQW exploits the path interference for efficient state transfer, and a certain phase difference in the initial superposition state, quantum walk with broken PTS is possible, similar to CQW. While the chiral character of CTQW is limited to certain initial states, this can still be practically significant when the implementation of CQW is a challenging and chiral transfer of arbitrary entangled states is not required.

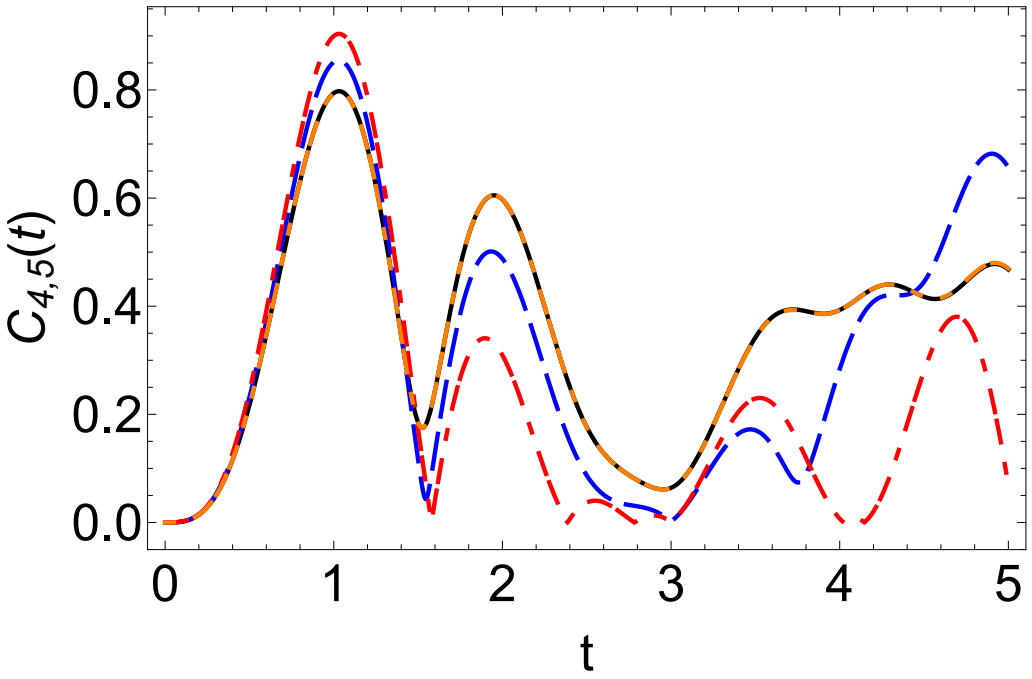


Figure 5: Time dependence of the concurrence $C_{4,5}$ measuring the pairwise entanglement between the sites $|4\rangle$ and $|5\rangle$ of a triangular chain of $N = 5$ sites over which an initial maximally entangled Bell state $(|1\rangle + |2\rangle)/\sqrt{2}$ of the sites 1 and 2 undergoes CQW. Different curves are for the different complex hopping coefficients of the CQW with the phases $\theta = \pi/4$ (solid, black), $\theta = \pm\pi/3$ (dashed, blue), $\theta = \pm\pi/2$ (dot-dashed-dashed, red), $\theta = \pm 3\pi/4$ (dot-dashed, orange); same as $\theta = \pi/4$.

3.2. PTS breaking and entanglement transfer in CQW on a triangular chain and comparison with CTQW

For CQW, we plot the concurrence in Fig. 5 by using an initial Bell state with $\phi = \pi$ in Eq. (5) and different θ in Eq. (3). We see that the concurrence is largest for $\theta = \pi/2$ with a value $C_{4,5}(1.02) \sim 0.9$, indicating that CQW has a slight time advantage ($\Delta t \sim 0.1$) along with a significantly higher quality transfer of entanglement compared to CTQW (cf. Fig. 3). Without plotting, we state here that a similar conclusion applies to occupation probabilities, too. We found that CQW with $\theta = \pi/2$ yields near perfect ($P_5 \sim 0.95$) state transfer $|1\rangle \to |5\rangle$ at $t \sim 1.64$.

We calculated the concurrences for $\phi = \pi/4$, $\phi = \pi/3$, $\phi = \pi/2$, $\phi = 3\pi/4$ and looked for the optimum θ values. We have found that for the state ($\phi = \pi$) initial Bell state, $\theta = \pi/2$ gives the optimum (maximum) concurrence $C_{4,5}(1.02) \sim 0.9$.

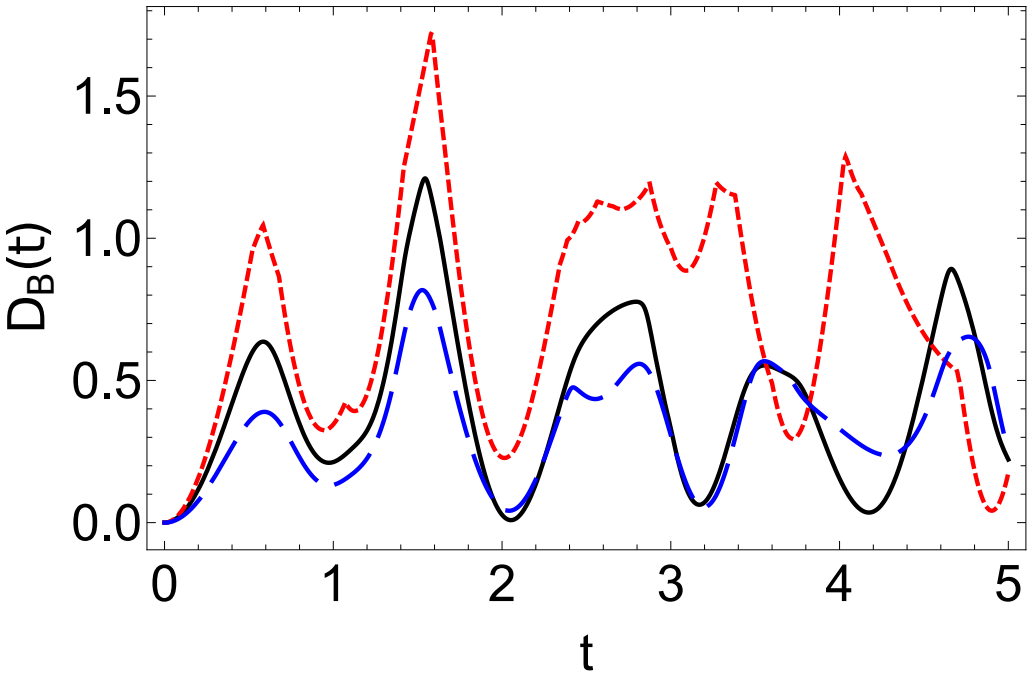


Figure 6: Time dependence of the Bures distance $D_B(t)$ between the diagonal elements of the forward and backward evolved density matrices $\rho(t)$ and $\rho(-t)$, respectively, for a CQW on a triangular chain of $N = 5$ sites. Initially the quantum walker is in a maximally entangled Bell state $(|1\rangle + |2\rangle)/\sqrt{2}$. Different curves are for chains with different complex hopping coefficients of phases $\theta = \pm\pi/4$ (dashed, blue), $\theta = \pm\pi/3$ (solid, black) and $\theta = \pm\pi/2$ (dotted, red). The Bures distance for the phases $\theta = 0$ and $\pm\pi$ are zero; and for $\theta = \pi/4$, $D_B(t)$ is the same as that of $\theta = 3\pi/4$.

We plot the Bures distance $D_B(t)$ for the diagonal elements of $\rho(t)$ and $\rho(-t)$ in Fig. 6, which shows that $D_B(t)$ is maximum for $\theta = \pm\pi/2$ (dotted, red). Remarkably, the maximum broken PTS in the CTQW is found for $\phi = \pi/2$. This suggests that $\phi = \theta = \pm\pi/2$ is an optimal choice for the broken-PTS condition both for CTQW and CQW over a triangular chain. The critical angle of maximum time-reversal asymmetry however coincides with a critical angle of optimum state transfer only for the CQW. When the numerical values of $D_B(t)$ for CTQW in Fig. 4 and CQW in Fig. 6 compared, $D_B(t)$ for CQW is numerically larger than CTQW, suggesting a larger broken PTS condition.

In Fig. 7, the concurrences for CQW and CTQW with an initial state of $(|1\rangle + |2\rangle)/\sqrt{2}$ are plotted. The solid red curve represents the CQW case and the dashed blue line is for the CTQW case. This plot also demonstrates the broken PTS in the CQW case. Here, one can notice the relatively higher entanglement

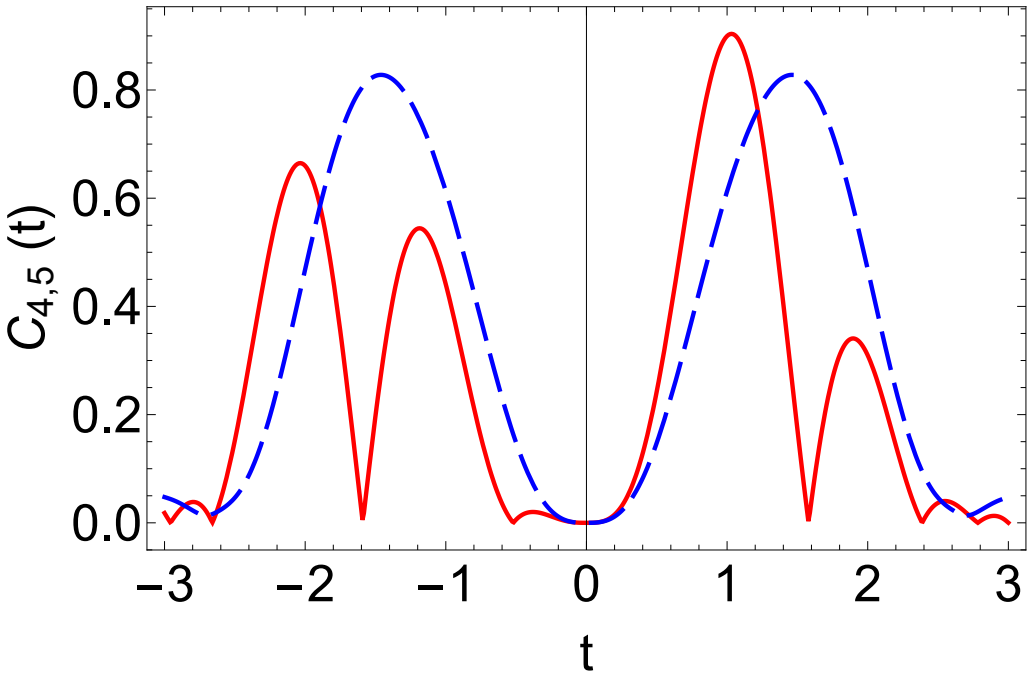


Figure 7: Time(t) dependence of the concurrence $C_{4,5}(t)$ to measure the entanglement between the sites $|4\rangle$ and $|5\rangle$ for an initially maximally entangled Bell state $(|1\rangle + |2\rangle)/\sqrt{2}$ of the sites $|1\rangle$ and $|2\rangle$ of a particle that makes CTQW (dashed, blue) and CQW (solid, red) with $\theta = \pi/2$ on a triangular chain of $N = 5$ sites. We take the phases of the complex hopping coefficients as $\theta = \pi/2$ for CQW; while for CTQW hopping coefficients are real with $\theta = 0$.

transfer quality in CQW. In addition, the transfer time is shorter in the case of CQW by $\Delta t \sim 0.4$.

To demonstrate the entanglement transfer in the short-time regime, we plot the dynamics of the concurrences $C_{i,j}$ that measure entanglement between every pair of sites (i, j) of the triangular chain in Fig. 8. One can see the transfer of entanglement from the sites $(|1\rangle, |2\rangle)$ to $(|4\rangle, |5\rangle)$. Although a spread over the sites is present, entanglement propagates mainly as $(|1\rangle, |2\rangle) \rightarrow (|2\rangle, |3\rangle) \rightarrow (|2\rangle, |4\rangle) \rightarrow (|3\rangle, |4\rangle) \rightarrow (|4\rangle, |5\rangle)$. If the success fidelity or the concurrence is sufficient, the entanglement can be collected at the end of the chain in this short-time regime. On the other hand, after multiple scatterings between the ends of the chain, the entanglement transfer can be enhanced at the cost of longer transfer time.

In Fig. 9, we plot the long-time behavior of the process for both CTQW and CQW. CQW demonstrates a higher concurrence peak in the short-time regime for the initial Bell state ($\phi = 0$). When the fidelities are considered, the longer-time

entanglement transfer fidelity is higher than the short-time regime's fidelities for CQW and CTQW. Both allow for PGST of the entanglement with $C_{4,5} = 0.999$ at $t = 28.1$ and with a concurrence of $C_{4,5} = 0.971$ at $t = 25.7$, respectively. These observations depend on the initial state and the chain size. Though not shown here, we numerically verified that CTQW gives a higher concurrence than CQW for certain initial conditions in the short-time regime (e.g., for $\phi = \pi/2$). Hence, we conclude that breaking PTS either by CQW for any initial condition or by CTQW for certain initial conditions gives comparable and high entanglement transfer performance in a short-time regime, which can be further enhanced to PGST in a long-time regime. The successful entanglement transfer (with a concurrence of more than 0.9) is limited to chains shorter than $N \sim 9$ sites, as discussed in Sec. 3.4.

3.3. Transfer of mixed Werner-States on the triangular chain

Having demonstrated the role of pure entangled states under the CQW scheme, it is natural to investigate the behavior of Werner-type mixed states under CQW with $\theta = \pi/2$ phase [75]. We introduce the Werner-like state

$$\rho_{\text{Werner}}(b) = b\rho(0) + (1-b)\rho_{\text{mixed}}, \tag{12}$$

where ρ_{mixed} is the maximally mixed state within the manifold of injection site states $|1\rangle$ and $|2\rangle$.

$$\rho_{\text{mixed}} = \frac{1}{2}\sum_{i=1}^{2} |i\rangle \langle i| . \tag{13}$$

We use the maximally entangled state within the manifold of injection site states, $|\psi(0)\rangle = (|1\rangle + |2\rangle)/\sqrt{2}$ to define the initial state density matrix $\rho(0) = |\psi_{\text{spatial}}(0)\rangle \langle\psi_{\text{spatial}}(0)|$.

To investigate the behaviour of entanglement transfer with respect to time, we calculate the fidelity $F(\rho(t), \rho_{\text{target}})$ as in Eq. (11) with the matrices $\rho(t)$ and ρ_{target}. Here, ρ_{target} represents the desired ideally transferred state

$$\rho_{\text{target}} = \frac{1}{2}\begin{bmatrix} 0 & 0 & 0 & 0 & 0 \\ 0 & 0 & 0 & 0 & 0 \\ 0 & 0 & 0 & 0 & 0 \\ 0 & 0 & 0 & 1 & b \\ 0 & 0 & 0 & b & 1 \end{bmatrix} . \tag{14}$$

In Fig. 10, we plot the time behavior of the Fidelity, $F(\rho(t), \rho_{\text{target}})$, for different b values. Clearly, the pure maximally entangled state $\rho_{\text{Werner}}(b = 1) = \rho(t = 0)$ yields the best entanglement transfer. On the contrary, fidelities closer to zero is observed at the maximally mixed state $\rho_{\text{Werner}}(b = 0) = \rho_{\text{mixed}}$.

3.4. *Scaling of entanglement transfer quality and time with respect to the chain size*

Until now, entanglement transfer on a chain of $N = 5$ sites has been discussed. In this subsection, we first investigate the entanglement transfer using CQW in the short-time regime by calculating the time $T_{\max}$ and value $C_{N-1,N}$ of the first peak of the concurrence for chains of up to $N = 71$ sites. Fig. 11a shows that $T_{\max}$ (which we refer to as transfer time) scales linearly with N, consistent with previous works [58, 59, 60]. Fig. 11b shows that the entanglement transfer quality decreases severely in chains longer than $N \sim 9$ sites. The figures include two different chiral phases θ values and indicate similar behavior.

Next, we explore the long-time entanglement transfer dynamics by assuming a waiting time of $t = 500$. In this case, we determine and fix an ideal value of θ for given N and initial state to find the maximum concurrence, which is not necessarily the first peak. The optimum θ for the initial state with $\phi = \pi$ is found to be $\pm\pi/2$, whose sign depends on N. The results are given in Table 1, which shows the maximum concurrence and when it occurs for given N and the corresponding optimum θ. For the same initial condition, the results for CTQW are presented in Table 2. While the tables report the results for the chains with up to $N = 33$ sites, the concurrence reduces to very low values after $N \sim 9$ sites. We can see that both CQW and CTQW methods to break PTS yield highly successful transfer of entangled states for relatively small graphs ($N < 9$). For such graphs (($N < 9$), CQW is faster than CTQW to transfer the entanglement, and its success is slightly higher (also cf. Fig. 7 where the same results are found for another initial condition ($\phi = 0$) and in the short-time regime).

4. Conclusion

We explored the transfer of spatial entanglement of a single spin excitation (which we call particle) undergoing either CQW or CTQW on a triangular chain. We found that particle transfer to the end of the chain is more successful if the particle is injected simultaneously from the leftmost pair of sites in a specific Bell-type superposition state. The success, measured by the rightmost site's occupation probability, depends on the relative phase ϕ between the site states in the initial quantum superposition. Using the Bures distance between the forward and backward time evolved states, we examined the dynamics of PTS breaking at different ϕ. We conclude that PTS breaking and the success of entangled state transfer via CTQW vary with ϕ. We explained the physical mechanism in terms of the role of the relative phase ϕ in the initial state played in the path interference in the triangular chain which eventually determines the quality of state transfer via

Chain Size N	Time (t)	Concurrence	Optimum Chiral Phase (θ)
5	55.4	0.999	$-\pi/2$
7	85.1	0.992	$\pi/2$
9	2.9	0.947	$-\pi/2$
11	321.3	0.900	$-\pi/2$
13	397.6	0.885	$-\pi/2$
15	4.5	0.874	$-\pi/2$
17	136.2	0.700	$-\pi/2$
19	68.6	0.714	$-\pi/2$
21	6.1	0.814	$-\pi/2$
23	416	0.635	$-\pi/2$
25	88.5	0.711	$-\pi/2$
27	7.7	0.764	$-\pi/2$
29	125.8	0.593	$\pi/2$
31	376.5	0.736	$\pi/2$
33	9.3	0.718	$-\pi/2$

Table 1: The maximum concurrence and the transfer time table for the longer-time CQW scenario $(t = 500)$ with the initial state phase $\phi = \pi$ along with the optimal phases for these parameters.

Chain Size N	Time (t)	Concurrence
5	193.9	0.993
7	342.8	0.979
9	410.6	0.900
11	482.7	0.805
13	498.3	0.749
15	288.2	0.748
17	82.5	0.697
19	4.1	0.661
21	4.5	0.631
23	4.9	0.608
25	5.3	0.594
27	5.7	0.581
29	6.1	0.567
31	6.4	0.552
33	6.8	0.540

Table 2: The maximum concurrence and the transfer time table for the longer-time CTQW scenario $(t = 500)$ with the initial state phase $\phi = \pi$.

CTQW. The success and PTS breaking character of CTQW is limited to certain initial states with strict initial phase values.

The chiral phase angle in CQW brings additional flexibility and generality to transfer arbitrary entangled states, which is not possible with CTQW. The chiral phase can be used to optimize transfer success. Even for those entangled states that can be transferred by CTQW, using optimum chiral phases, entanglement transfer with CQW is found to be faster and more successful for small graphs with less than 9 sites. In our examinations, we also considered long chains (about 70 sites). When longer triangular chains are considered, the entanglement transfer success is severely reduced for both CQW and CTQW.

We examined both short-time and long-time dynamics of entanglement transfer. In the short-time regime, the first peak of the concurrence is used to probe the entanglement transfer. The time when the first peak emerges (entanglement transfer time) scales linearly with the chain size, as expected from the earlier works [58, 59, 60]. Longer-time regime is used to look for a global maximum in entanglement dynamics, and hence it can give higher entanglement transfer success at the cost of longer waiting times. Speed and success advantages of CQW over CTQW for certain initial states remain in the longer-time regime as well. Breaking PTS strongly either by CQW for any initial condition or by CTQW for certain initial conditions give comparable and high entanglement transfer performance in a short-time regime, which can be further enhanced in long-time regime; though short-time regime can be more practical for real applications open to environmental quantum decoherence effects.

In summary, if CTQW is capable to transfer entanglement with PTS breaking for a certain initial state, then the performance of transfer is comparable to CQW. Hence, if implementing CQW is challenging and transfer of arbitrary entangled states is not required, we conclude that CTQW can be preferred over CQW. On the other hand, if the optimum transfer of arbitrary entangled states with PTS breaking character is required than it is necessary to implement CQW. Our main conclusion is foundational in nature, based upon the physical mechanism of PTS breaking in terms of the path interference and phases in the initial state and hopping coefficients, and hence, is independent of any physical embodiment.

In addition, we explored the behavior of various mixed Werner states under our CQW scheme. We found that the purest maximally entangled state yields the best state transfer.

Our results can help to understand the interplay of PTS breaking and entanglement transfer and practically to design optimum chiral lattices for the transfer of entangled states in physical platforms such as plasmonic non-Hermitian coupled

waveguides [69], ultracold atomic optical lattices [65], photonic-spin waveguides [64], or quantum superconducting circuits [61, 62].

5. Acknowledgements

The authors thank Tony John George Apollaro and Deniz N. Bozkurt for fruitful discussions.

Appendix A Perfect state and entanglement transfer on circulant graphs

We present perfect state and entanglement transfer on some circulant graphs in this appendix. Such graphs occupy a relatively large space than linear triangular chains to transfer a state over the same distance and require more qubits to implement. For example, we take a 5×5 circulant graph shown in Fig.12a with only nearest-neighbor interactions. The adjacency matrix for such a graph is

$$A = \begin{bmatrix} 0 & -\mathrm{i} & 0 & 0 & -\mathrm{i} \\ \mathrm{i} & 0 & -\mathrm{i} & 0 & 0 \\ 0 & \mathrm{i} & 0 & -\mathrm{i} & 0 \\ 0 & 0 & \mathrm{i} & 0 & -\mathrm{i} \\ \mathrm{i} & 0 & 0 & \mathrm{i} & 0 \end{bmatrix}. \tag{15}$$

Fig. 13 shows that the entanglement transfer on such a graph is nearly perfect with a concurrence of $C \sim 0.93$ at $t \sim 4.5$.

Another example is a pentagram graph which is sketched on Fig.12b. This graph contains three triangular plaquettes, but being circulant comes with the cost of more edges. The adjacency matrix reads

$$A = \begin{bmatrix} 0 & -\mathrm{i} & -\mathrm{i} & -\mathrm{i} & -\mathrm{i} \\ \mathrm{i} & 0 & -\mathrm{i} & -\mathrm{i} & -\mathrm{i} \\ \mathrm{i} & \mathrm{i} & 0 & -\mathrm{i} & -\mathrm{i} \\ \mathrm{i} & \mathrm{i} & \mathrm{i} & 0 & -\mathrm{i} \\ \mathrm{i} & \mathrm{i} & \mathrm{i} & \mathrm{i} & 0 \end{bmatrix}. \tag{16}$$

Fig. 14 presents the possibility of nearly perfect entanglement transfer with a concurrence of $C_{4,5} \sim 1$ at $t \sim 3.7$.

Appendix B Eigenvalues and Eigenstates of the Hamiltonian

The eigenstates corresponding to the eigenvalues in Eq. (4), are listed in the same order as the equations,

$$\Lambda_1 = \begin{bmatrix} -0.65 - 0.76\mathrm{i} \\ -0.65 + 0.76\mathrm{i} \\ 0.22 + 0.98\mathrm{i} \\ 0.22 - 0.98\mathrm{i} \\ 0 \end{bmatrix}, \Lambda_2 = \begin{bmatrix} 0.65 + 1.15\mathrm{i} \\ 0.65 - 1.15\mathrm{i} \\ -0.22 + 0.50\mathrm{i} \\ , -0.22 - 0.50\mathrm{i} \\ 1 \end{bmatrix},$$
$$\Lambda_3 = \begin{bmatrix} 1 \\ 1 \\ 1 \\ 1 \\ 0 \end{bmatrix}, \Lambda_4 = \begin{bmatrix} -0.65 + 1.40\mathrm{i} \\ -0.65 - 1.40\mathrm{i} \\ 0.22 + 0.18\mathrm{i} \\ 0.22 - 0.18\mathrm{i} \\ -1\mathrm{i} \end{bmatrix}, \Lambda_5 = \begin{bmatrix} -1.30 + 0.25\mathrm{i} \\ -1.30 - 0.25\mathrm{i} \\ 0.44 - 0.33\mathrm{i} \\ 0.445 + 0.33\mathrm{i} \\ 1 \end{bmatrix}. \quad (17)$$

Appendix C Definitions of the some mathematical and graph theory terms used in the manuscript

A graph is a set of vertices and edges connecting them. Here, we present definitions of some mathematical terms from graph theory and linear algebra we used in the main text.
Hadamard Product:Hadamard Product is the element-wise product of two matrices with the same dimensions.

Circulant Graph:Undirected graphs contain only bidirectional edges. Circulant graphs are undirected graphs, which take any vertex to all of the other vertices .

Flat Eigenbasis:When each eigenvector of a basis has entries of the same magnitude, that eigenbasis is called a flat eigenbasis [39].

Adjacency Matrix, and the Graph Laplacian Matrix:A Laplacian matrix $L = D - A$ is a matrix that describes a graph, where A is the adjacency matrix and D is the degree matrix. A degree matrix is a diagonal matrix whose elements indicate the number of edges attached to each vertex of a graph. An adjacency matrix represents the connections of a graph, whose elements corresponding to adjacent (connected by an edge) vertices are 1 [76].

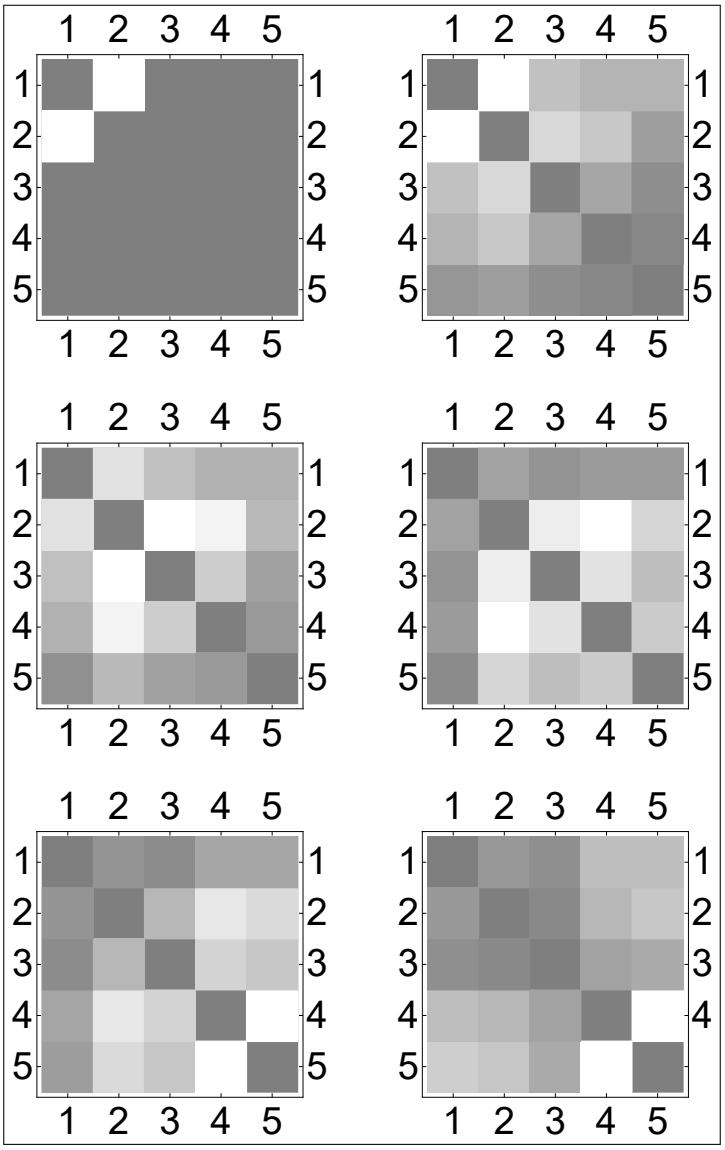


Figure 8: The time evolution of concurrence $C_{i,j}$, measuring the pairwise entanglement between the sites $|i\rangle$ and $|j\rangle$, is shown as a matrix with $i, j = 1..5$. Each square in these matrices stands for the value of the concurrence $C_{i,j}$. Colors from light to dark scale with 1 to 0, respectively. Initially (at $t = 0$), the quantum walker is injected in the maximally entangled Bell state of the sites 1 and 2 with $C_{1,2} = 1$ (upper left panel) to undergo CQW with complex hopping coefficients with phase $\theta = \pi/2$. As time progresses, one can notice the unidirectional transfer of entanglement (light colored pair of squares) to the rightmost sites 4 and 5. The panels are for the $t = 0$ (upper left), $t = 0.2$ (upper right), $t = 0.4$ (middle left), $t = 0.6$ (middle right), $t = 0.8$ (bottom left), and $t = 1$ (bottom right).

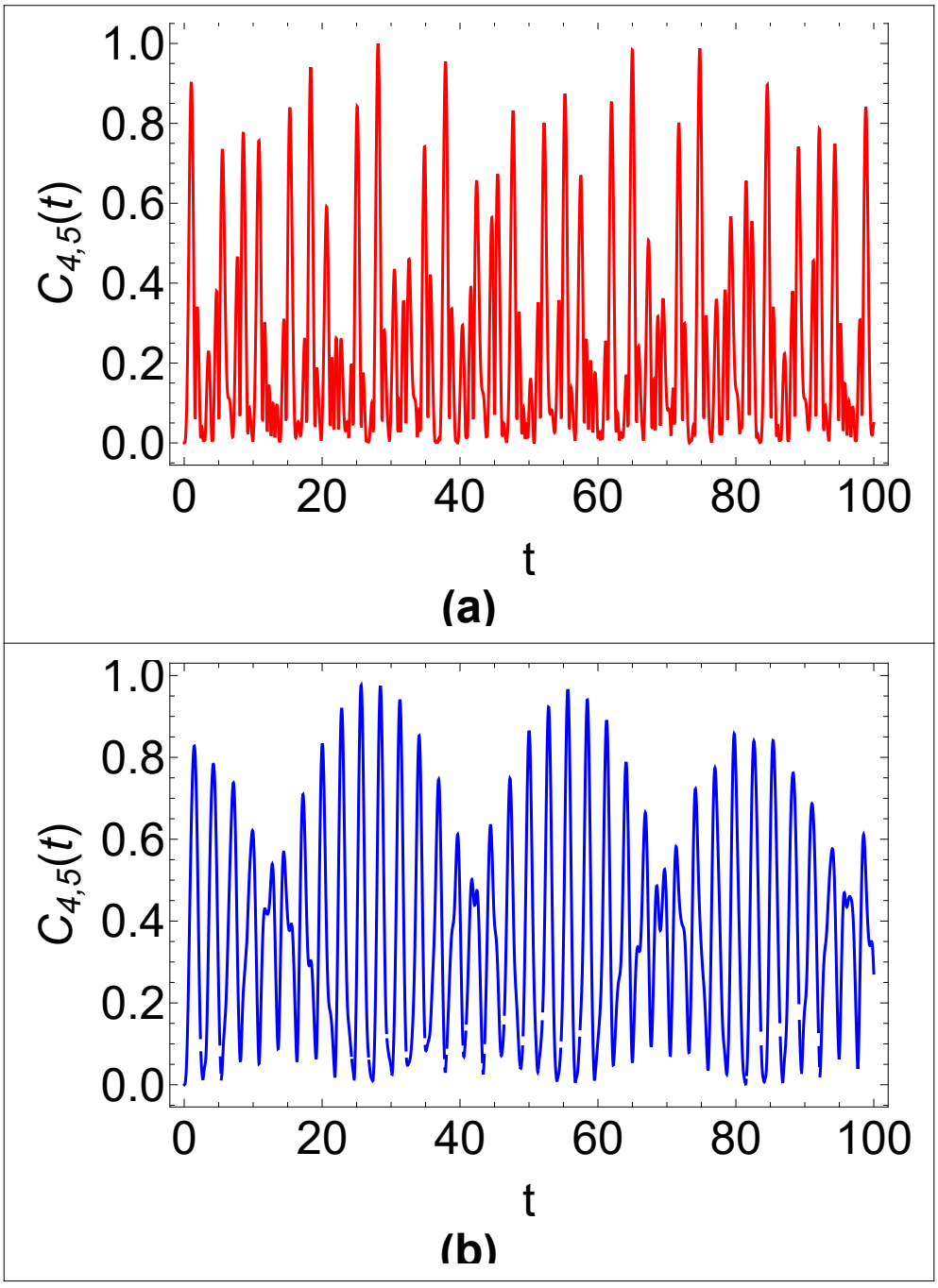


Figure 9: Time dependence of the concurrence $C_{4,5}(t)$ of CQW (solid blue curve) and CTQW (solid red curve) for the long-time evolution $(t = 0 - 100)$. In this plot, we have considered the initial state $|\psi_{\text{spatial}}(0)\rangle = (|1\rangle + |2\rangle)/\sqrt{2}$.

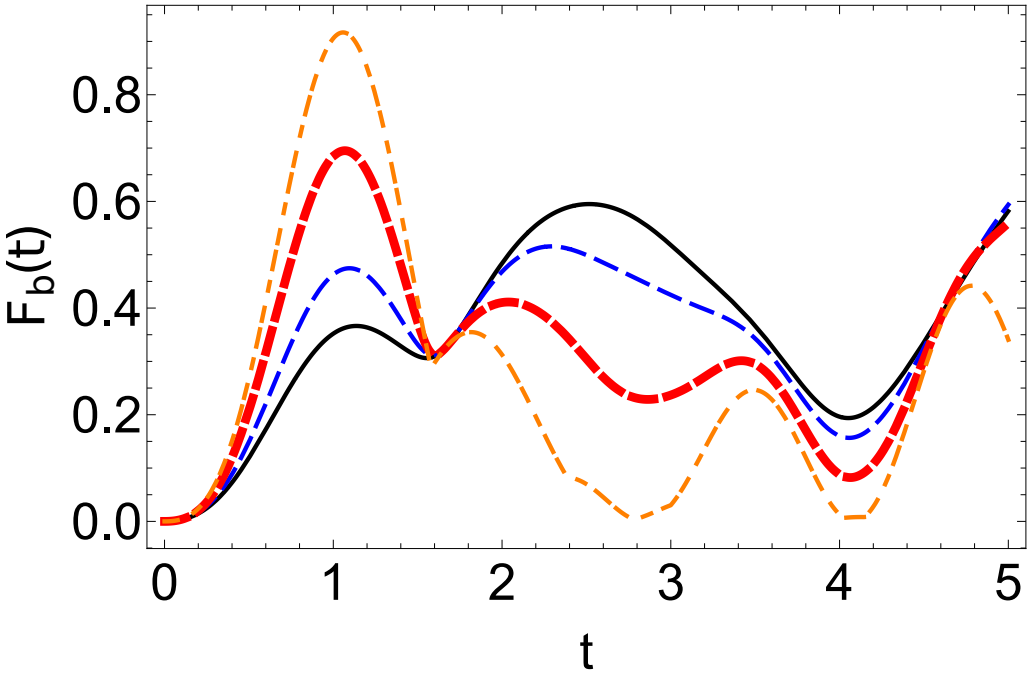
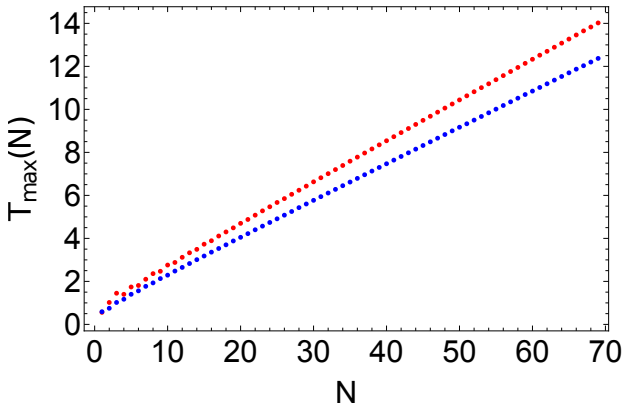
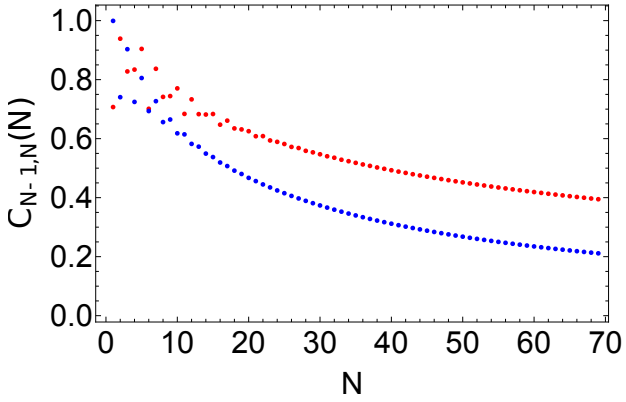


Figure 10: Time dependence of the Fidelity $F(\rho(t), \rho_{\text{target}})$ between $\rho(t)$ and ρ_{Werner} as a function of time t with an initial Werner state under the scheme of CQW on a triangular chain of $N = 5$ sites with complex edge weights of phase $\theta = \pi/2$. Where $b = -1/4$ as solid black, $b = 0$ as dashed blue, $b = 1/2$ as thick dashed red and finally, maximally entangled bell state $b = 1$ is dot-dashed orange.

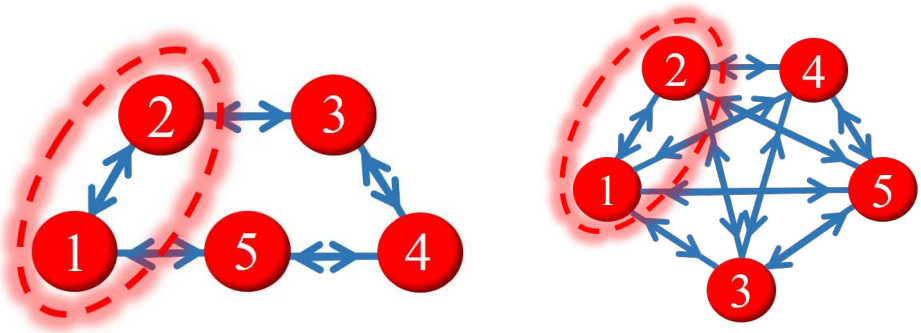


(a)



(b)

Figure 11: **(a)** Scaling of state transfer time with respect to the chain size. Red dots represent $\theta = 0$ and blue dots represent $\theta = \pi/2$ **(b)** Concurrence value at the state transfer time. Red dots represent $\theta = 0$ and blue dots represent $\theta = \pi/2$



(a) (b)

Figure 12: **(a)** Graph of a linear chain of 5 vertices arranged as an odd number cycle. **(b)** Graph of a linear chain of 5 vortices arranged as a pentagram with five-pointed star-like diagonal connections.

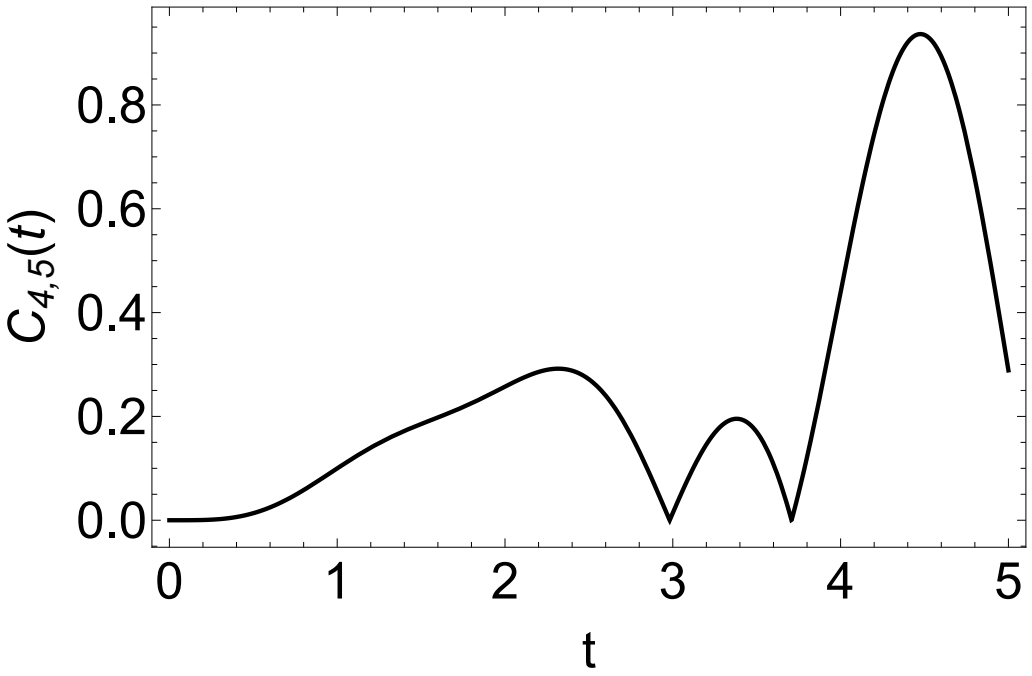


Figure 13: Time(t) dependence of the concurrence $C_{4,5}(t)$ to measure the entanglement between the sites $|4\rangle$ and $|5\rangle$ on a 5×5 circulant graph with only nearest-neighbour interactions for an initially maximally entangled Bell state $(|1\rangle + |2\rangle)/\sqrt{2}$ of the sites $|1\rangle$ and $|2\rangle$ of a particle that makes CQW.

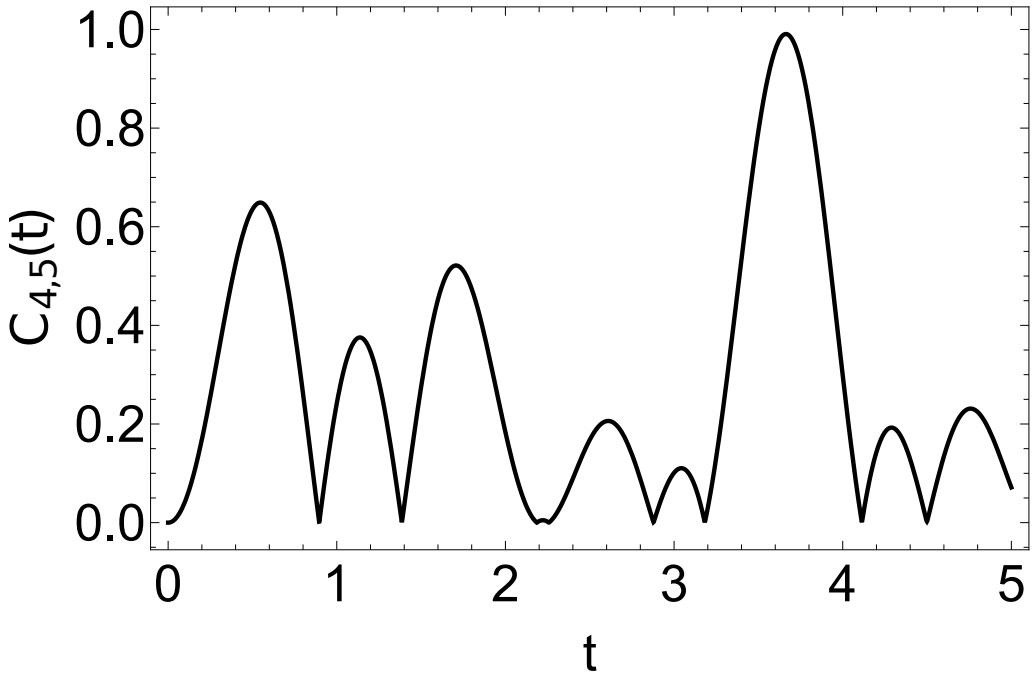


Figure 14: Time(t) dependence of the concurrence $C_{4,5}(t)$ to measure the entanglement between the sites $|4\rangle$ and $|5\rangle$ on a complete pentagram graph for an initially maximally entangled Bell state $(|1\rangle + |2\rangle)/\sqrt{2}$ of the sites $|1\rangle$ and $|2\rangle$ of a particle that makes CQW.

6. References

References

[1] Charles H. Bennett and David P. DiVincenzo. Quantum information and computation. *Nature*, 404(6775):247–255, March 2000.

[2] David P. DiVincenzo. The Physical Implementation of Quantum Computation. *Fortschritte der Phys.*, 48(9-11):771–783, 2000.

[3] H. J. Kimble. The quantum internet. *Nature*, 453(7198):1023–1030, June 2008.

[4] Sougato Bose. Quantum Communication through an Unmodulated Spin Chain. *Phys. Rev. Lett.*, 91(20):207901, November 2003.

[5] Matthias Christandl, Nilanjana Datta, Artur Ekert, and Andrew J. Landahl. Perfect State Transfer in Quantum Spin Networks. *Phys. Rev. Lett.*, 92(18):187902, May 2004.

[6] Claudio Albanese, Matthias Christandl, Nilanjana Datta, and Artur Ekert. Mirror Inversion of Quantum States in Linear Registers. *Phys. Rev. Lett.*, 93(23):230502, November 2004.

[7] Antoni Wójcik, Tomasz Łuczak, Paweł Kurzyński, Andrzej Grudka, Tomasz Gdala, and Małgorzata Bednarska. Unmodulated spin chains as universal quantum wires. *Phys. Rev. A*, 72(3):034303, September 2005.

[8] C. Di Franco, M. Paternostro, and M. S. Kim. Perfect State Transfer on a Spin Chain without State Initialization. *Phys. Rev. Lett.*, 101(23):230502, December 2008.

[9] Masoud Mohseni, Patrick Rebentrost, Seth Lloyd, and Alán Aspuru-Guzik. Environment-assisted quantum walks in photosynthetic energy transfer. *J. Chem. Phys.*, 129(17):174106, November 2008.

[10] T. J. G. Apollaro, L. Banchi, A. Cuccoli, R. Vaia, and P. Verrucchi. 99$%$-fidelity ballistic quantum-state transfer through long uniform channels. *Phys. Rev. A*, 85(5):052319, May 2012.

[11] I. Sinayskiy, A. Marais, F. Petruccione, and A. Ekert. Decoherence-Assisted Transport in a Dimer System. *Phys. Rev. Lett.*, 108(2):020602, January 2012.

[12] Kamil Korzekwa, Paweł Machnikowski, and Paweł Horodecki. Quantum-state transfer in spin chains via isolated resonance of terminal spins. *Phys. Rev. A*, 89(6):062301, June 2014.

[13] Marta P. Estarellas, Irene D'Amico, and Timothy P. Spiller. Robust quantum entanglement generation and generation-plus-storage protocols with spin chains. *Phys. Rev. A*, 95(4):042335, April 2017.

[14] Tao Shi, Ying Li, Zhi Song, and Chang-Pu Sun. Quantum-state transfer via the ferromagnetic chain in a spatially modulated field. *Phys. Rev. A*, 71(3):032309, March 2005.

[15] M. J. Hartmann, M. E. Reuter, and M. B. Plenio. Excitation and entanglement transfer versus spectral gap. *New J. Phys.*, 8(6):94–94, June 2006.

[16] L. Banchi, T. J. G. Apollaro, A. Cuccoli, R. Vaia, and P. Verrucchi. Optimal dynamics for quantum-state and entanglement transfer through homogeneous quantum systems. *Phys. Rev. A*, 82(5):052321, November 2010.

[17] H. J. Shan, C. M. Dai, H. Z. Shen, and X. X. Yi. Controlled state transfer in a Heisenberg spin chain by periodic drives. *Sci. Rep*, 8(1):13565, September 2018.

[18] Zhi He, Chunmei Yao, and Jian Zou. Robust state transfer in the quantum spin channel via weak measurement and quantum measurement reversal. *Phys. Rev. A*, 88(4):044304, October 2013.

[19] Zhong-Xiao Man, Nguyen Ba An, Yun-Jie Xia, and Jaewan Kim. Controllable entanglement transfer via two parallel spin chains. *Phys. Lett. A*, 378(30):2063–2069, June 2014.

[20] Analia Zwick, Gonzalo A. Álvarez, Guy Bensky, and Gershon Kurizki. Optimized dynamical control of state transfer through noisy spin chains. *New J. Phys.*, 16(6):065021, June 2014.
[21] Dong-Xiao Li, Dong-Xiao Li, Xian-Miao Liao, Xian-Miao Liao, Xiao-Qiang Shao, and Xiao-Qiang Shao. One-way quantum state transfer in a lossy coupled-cavity array. *Opt. Express*, 27(24):35971–35980, November 2019.
[22] Yuichiro Matsuzaki, Victor M. Bastidas, Yuki Takeuchi, William J. Munro, and Shiro Saito. One-way Transfer of Quantum States via Decoherence. *J. Phys. Soc. Japan*, 89(4):044003, March 2020.
[23] Rafael Vieira and Gustavo Rigolin. Almost perfect transmission of multipartite entanglement through disordered and noisy spin chains. *Phys. Lett. A*, 384(22):126536, August 2020.
[24] Wai-Keong Mok, Davit Aghamalyan, Jia-Bin You, Tobias Haug, Wenzu Zhang, Ching Eng Png, and Leong-Chuan Kwek. Long-distance dissipation-assisted transport of entangled states via a chiral waveguide. *Phys. Rev. Res.*, 2:013369, Mar 2020.
[25] Gabriele De Chiara, Davide Rossini, Simone Montangero, and Rosario Fazio. From perfect to fractal transmission in spin chains. *Phys. Rev. A*, 72(1):012323, July 2005.
[26] S. Ashhab. Quantum state transfer in a disordered one-dimensional lattice. *Phys. Rev. A*, 92(6):062305, December 2015.
[27] Zhong-Xiao Man, Nguyen Ba An, Yun-Jie Xia, and Jaewan Kim. Controllable entanglement transfer via two parallel spin chains. *Physics Letters A*, 378(30-31):2063–2069, June 2014.
[28] L. Campos Venuti, S. M. Giampaolo, F. Illuminati, and P. Zanardi. Long-distance entanglement and quantum teleportation in xx spin chains. *Phys. Rev. A*, 76:052328, Nov 2007.
[29] L Banchi, T J G Apollaro, A Cuccoli, R Vaia, and P Verrucchi. Long quantum channels for high-quality entanglement transfer. *New Journal of Physics*, 13(12):123006, dec 2011.
[30] Giulia Gualdi, Vojtech Kostak, Irene Marzoli, and Paolo Tombesi. Perfect state transfer in long-range interacting spin chains. *Phys. Rev. A*, 78:022325, Aug 2008.
[31] Salvatore M Giampaolo and Fabrizio Illuminati. Long-distance entanglement in many-body atomic and optical systems. *New Journal of Physics*, 12(2):025019, feb 2010.
[32] Zhong-Xiao Man, Nguyen Ba An, Yun-Jie Xia, and Jaewan Kim. Universal scheme for finite-probability perfect transfer of arbitrary multispin states through spin chains. *Annals of Physics*, 351:739–750, December 2014.
[33] Oliver Mülken and Alexander Blumen. Continuous-time quantum walks: Models for coherent transport on complex networks. *Phys. Rep.*, 502(2):37 – 87, 2011.
[34] Andris Ambainis. Quantum walks and their algorithmic applications. *Int. J. Quantum Inf.*, 01(04):507–518, 2003.
[35] Xiang Zhan, Hao Qin, Zhi-hao Bian, Jian Li, and Peng Xue. Perfect state transfer and efficient quantum routing: A discrete-time quantum-walk approach. *Phys. Rev. A*, 90(1):012331, July 2014.
[36] M. Štefaňák and S. Skoupý. Perfect state transfer by means of discrete-time quantum walk search algorithms on highly symmetric graphs. *Phys. Rev. A*, 94(2):022301, August 2016.
[37] Vivien M. Kendon and Christino Tamon. Perfect State Transfer in Quantum Walks on Graphs. *J. Comput. Theor. Nanosci.*, 8(3):422–433, March 2011.
[38] Steven J. Large, Michael S. Underwood, and David L. Feder. Perfect quantum state transfer of hard-core bosons on weighted path graphs. *Phys. Rev. A*, 91(3):032319, March 2015.
[39] Stephen Cameron, Shannon Fehrenbach, Leah Granger, Oliver Hennigh, Sunrose Shrestha, and Christino Tamon. Universal state transfer on graphs. *Linear Algebra Appl.*, 455:115–142,

August 2014.

[40] Erin Connelly, Nathaniel Grammel, Michael Kraut, Luis Serazo, and Christino Tamon. Universality in perfect state transfer. *Linear Algebra Appl.*, 531:516–532, October 2017.

[41] Zoltán Zimborás, Mauro Faccin, Zoltán Kádár, James D. Whitfield, Ben P. Lanyon, and Jacob Biamonte. Quantum transport enhancement by time-reversal symmetry breaking. *Sci. Rep*, 3(1), August 2013.

[42] Dawei Lu, Jacob D. Biamonte, Jun Li, Hang Li, Tomi H. Johnson, Ville Bergholm, Mauro Faccin, Zoltán Zimborás, Raymond Laflamme, Jonathan Baugh, and Seth Lloyd. Chiral quantum walks. *Phys. Rev. A*, 93:042302, Apr 2016.

[43] Thomas G Wong. Quantum walk search with time-reversal symmetry breaking. *J. Phys. A Math. Theor.*, 48(40):405303, September 2015.

[44] Yang Liu and D. L. Zhou. Quantum state transfer along a ring with time-reversal asymmetry. *Phys. Rev. A*, 91(5):052318, May 2015.

[45] Daniele Cozzolino, Beatrice Da Lio, Davide Bacco, and Leif Katsuo Oxenløwe. High-dimensional quantum communication: Benefits, progress, and future challenges. *Adv. Quantum Technol.*, 2(12):1900038, October 2019.

[46] X. S. Liu, G. L. Long, D. M. Tong, and Feng Li. General scheme for superdense coding between multiparties. *Phys. Rev. A*, 65(2), January 2002.

[47] Andrzej Grudka and Antoni Wójcik. Symmetric scheme for superdense coding between multiparties. *Phys. Rev. A*, 66(1), July 2002.

[48] Xiao Min Hu, Yu Guo, Bi Heng Liu, Yun Feng Huang, Chuan Feng Li, and Guang Can Guo. Beating the channel capacity limit for superdense coding with entangled ququarts. *Sci. Adv.*, 4(7), July 2018.

[49] ALASTAIR KAY. PERFECT, EFFICIENT, STATE TRANSFER AND ITS APPLICATION AS a CONSTRUCTIVE TOOL. *International Journal of Quantum Information*, 08(04):641–676, June 2010.

[50] Alastair Kay and Marie Ericsson. Geometric effects and computation in spin networks. *New Journal of Physics*, 7:143–143, June 2005.

[51] Taira Giordani, Luca Innocenti, Alessia Suprano, Emanuele Polino, Mauro Paternostro, Nicolò Spagnolo, Fabio Sciarrino, and Alessandro Ferraro. Entanglement transfer, accumulation and retrieval via quantum-walk-based qubit–qudit dynamics. *New Journal of Physics*, 23(2):023012, February 2021.

[52] Sandeep K Goyal and C M Chandrashekar. Spatial entanglement using a quantum walk on a many-body system. *Journal of Physics A: Mathematical and Theoretical*, 43(23):235303, May 2010.

[53] Stefano Azzini, Sonia Mazzucchi, Valter Moretti, Davide Pastorello, and Lorenzo Pavesi. Single-particle entanglement. *Advanced Quantum Technologies*, 3(10):2000014, September 2020.

[54] William K. Wootters. Entanglement of formation of an arbitrary state of two qubits. *Phys. Rev. Lett.*, 80:2245–2248, Mar 1998.

[55] Richard Jozsa. Fidelity for mixed quantum states. *J. Mod. Opt*, 41(12):2315–2323, December 1994.

[56] Matthias Hübner. Explicit computation of the bures distance for density matrices. *Phys. Lett. A*, 163(4):239–242, March 1992.

[57] Matthias Hübner. Computation of uhlmann's parallel transport for density matrices and the bures metric on three-dimensional hilbert space. *Phys. Lett. A*, 179(4-5):226–230, August

1993.

[58] S. Lorenzo, T. J. G. Apollaro, S. Paganelli, G. M. Palma, and F. Plastina. Transfer of arbitrary two-qubit states via a spin chain. *Phys. Rev. A*, 91:042321, Apr 2015.

[59] Wayne Jordan Chetcuti, Claudio Sanavio, Salvatore Lorenzo, and Tony J G Apollaro. Perturbative many-body transfer. *New Journal of Physics*, 22(3):033030, mar 2020.

[60] Salvatore Lorenzo, Tony J. G. Apollaro, Andrea Trombettoni, and Simone Paganelli. 2-qubit quantum state transfer in spin chains and cold atoms with weak links. *International Journal of Quantum Information*, 15(05):1750037, August 2017.

[61] Antti Vepsäläinen and Gheorghe Sorin Paraoanu. Simulating spin chains using a superconducting circuit: Gauge invariance, superadiabatic transport, and broken time-reversal symmetry. *Adv. Quantum Technol.*, 3(4):1900121, April 2020.

[62] Ken K. W. Ma. Multiphoton resonance and chiral transport in the generalized rabi model. *Phys. Rev. A*, 102(5), November 2020.

[63] Tom Manovitz, Yotam Shapira, Nitzan Akerman, Ady Stern, and Roee Ozeri. Quantum simulations with complex geometries and synthetic gauge fields in a trapped ion chain. *PRX Quantum*, 1:020303, Oct 2020.

[64] Tomás Ramos, Benoît Vermersch, Philipp Hauke, Hannes Pichler, and Peter Zoller. Non-markovian dynamics in chiral quantum networks with spins and photons. *Phys. Rev. A*, 93:062104, Jun 2016.

[65] Jiannis K. Pachos and Martin B. Plenio. Three-spin interactions in optical lattices and criticality in cluster hamiltonians. *Phys. Rev. Lett.*, 93:056402, Jul 2004.

[66] Immanuel Bloch, Jean Dalibard, and Wilhelm Zwerger. Many-body physics with ultracold gases. *Rev. Mod. Phys.*, 80(3):885–964, July 2008.

[67] Monika Aidelsburger, Sylvain Nascimbene, and Nathan Goldman. Artificial gauge fields in materials and engineered systems. *CR PHYS*, 19(6):394–432, September 2018.

[68] E. K. Levi, P. G. Kirton, and B. W. Lovett. Designing spin-channel geometries for entanglement distribution. *Phys. Rev. A*, 94:032302, Sep 2016.

[69] Ziwei Fu, Nianzu Fu, Huaiyuan Zhang, Zhe Wang, Dong Zhao, and Shaolin Ke. Extended SSH model in non-hermitian waveguides with alternating real and imaginary couplings. *Appl. Sci.*, 10(10):3425, May 2020.

[70] J Kempe. Quantum random walks: An introductory overview. *Contemp. Phys.*, 44(4):307–327, July 2003.

[71] A. Sett, H. Pan, P. E. Falloon, and J. B. Wang. Zero transfer in continuous-time quantum walks. *Quantum Inf. Process.*, 18(5), April 2019.

[72] Edward Farhi and Sam Gutmann. Quantum computation and decision trees. *Phys. Rev. A*, 58:915–928, Aug 1998.

[73] Andrew M. Childs, Edward Farhi, and Sam Gutmann. *Quantum Inf. Process.*, 1(1/2):35–43, 2002.

[74] Isaac L. Chuang Michael A. Nielsen. *Quantum Computation and Quantum Information*. Cambridge University Press, Cambridge, 2010.

[75] Reinhard F. Werner. Quantum states with einstein-podolsky-rosen correlations admitting a hidden-variable model. *Physical Review A*, 40(8):4277–4281, 1989.

[76] F. Chung, L. Lu, and V. Vu. Spectra of random graphs with given expected degrees. *Proceedings of the National Academy of Sciences*, 100(11):6313–6318, May 2003.